Journal of Smart Sensor and Materials
Volume 1, 2023, No 3 (2023)

CARBON DOTS-SILVER BASED FLUORESCENCE ASSAY FOR THE DETECTION OF *Escherichia coli* O157:H7

Suria Mohd Saad[1,2,*], Jaafar Abdullah[2,3], Suraya Abd Rashid[2], Yap Wing Fen[4], Faridah Salam[1] and Lau Han Yih[1]

[1] Biotechnology and Nanotechnology Research Centre, MARDI Headquarters, Persiaran MARDI-UPM, 43400 Serdang, Selangor, Malaysia
[2] Institute of Nanoscience and Nanotechnology, University Putra Malaysia, 43400 Serdang, Selangor, Malaysia
[3] Department of Chemistry, Faculty of Science, University Putra Malaysia, 43400 Serdang, Selangor, Malaysia
[4] Department of Physics, Faculty of Science, University Putra Malaysia, 43400 Serdang, Selangor, Malaysia
[*]*Corresponding author: suria@mardi.gov.my*

ABSTRACT

The detection of *Escherichia coli* O157:H7 (*E. coli* O157:H7) from various food matrices is important in the clinical field for the diagnosis of diseases. To identify the *E. coli* O157:H7 *fliC* gene; carbon dots (CDs), fluorophore-oligonucleotide, silver nanoparticles (AgNPs), quencher-oligonucleotide and target oligonucleotide were incorporated into the fabrication of single fluorescent sensor. The sensor works based on the principle of fluorescence quenching between CDs and AgNPs when the target oligonucleotide is co-hybridized with oligonucleotide on the surface of CDs (fluorophore) and AgNPs (quencher), respectively. AgNPs acts as a quencher by *in situ* absorption of CDs energy in the presence of target oligonucleotide. When the sensing system is excited at 340 nm, the optimum emission at 450 nm, corresponding to CDs emission, appears and the interaction between CDs as fluorophore and AgNPs as quencher indicates the presence of fluorescence quenching. Fluorophore emission was triggered inversely proportional to the change in target concentration. The linear calibration plot towards target oligonucleotide was obtained in the dilution series from 0.001 nM to 200 nM with a detection limit (LOD) of 0.0088 ± 0.71 nM. The results of kinetic studies using fluorescence assay found a strong relationship and interaction between fluorophore and quencher.

Keywords: Fluoresence assay, Stern-Volmer constant, Association constant, Binding constant

INTRODUCTION

Carbon dots (CDs) are bright luminous nanoparticles (NPs). A large number of insights of the optical properties of CDs have recently been studied in various aspects such as nanotechnology architectures [1], FRET design [2], fluorescence sensing [3], synthesis, properties and even applications [4]. In addition, CDs has also been explored in detection of biomarkers of various diseases because its fluorescence properties are easily adjusted in the visible spectrum and integrated into polymer microbeads [5]. A large amount of research aims to determine the electronic properties and potential uses of CDs, growing at a rapid rate, due to its excellent conductivity, electronic and optical properties [3].

Fluorescence is a physical phenomenon in which fluorochrome (a chemical compound) emits light at a certain wavelength shortly after it is excited by light at another wavelength [6]. Meanwhile, fluorescent quenching refers to the process of various

molecular interactions, such as the formation of ground state complexes, molecular rearrangements, electron transfer, excited state reactions and collisional quenching that cause a decrease in sample fluorescence intensity. One of the most popular equations used to study fluorescent quenching is the Stern-Volmer equation (1).

$$\frac{F_0}{F} = 1 + K_{SV}[Q] \qquad (1)$$

where F_0 and F are the fluorescent intensities without and with quencher, respectively. $[Q]$ is the quencher concentration and K_{SV} is the Stern-Volmer constant derived from the linear plot slope F_0/F relative to $[Q]$. Fluorescence quenching is one of the techniques used in the development of biosensors that offers several advantages such as high sensitivity, relatively able to detect at low levels, avoiding the use of radioactive materials, etc.

Advances in diagnostic biosensor technology are growing rapidly. Many are interested in using silver nanoparticles (AgNPs) to improve or replace materials used in conventional sensing technology. AgNPs have advantages over other materials in conventional diagnostics, as they can be engineered to possess certain properties or behave in certain ways [7]. AgNPs metal surfaces can alter fluorescent free-space conditions with spectral properties that can result in dramatic spectral changes [8]. Due to the advantages of surface characteristics and high particle stability, AgNPs have been widely studied as a fluorescent quencher [9]. Noble metal nanoparticles such as gold (Au) and silver (Ag) have been explored regarding their synthesis in most metal nanostructure research [10]. Previously, Ag nanoclusters, consisting of several silver atoms, have gained attention for DNA detection due to their simple synthesis, convincing luminescence and biocompatibility [11].

In recent years, serious threats to public health around the world have emerged as a result of food safety issues. Consuming food contaminated with foodborne pathogens can affect the human body [12]. *Escherichia coli* O157:H7 (*E. coli* O157:H7), a foodborne pathogen, has been identified and is often reported as a significant threat to human health [13]. The most widely used method to detect *E. coli* O157:H7 is the sandwich enzyme-linked immunosorbent assay (ELISA) because of its accuracy and inexpensiveness, but this method is limited by its sensitivity [14]. Therefore, analytical methods to detect *E. coli* O157:H7 with sensitivity, accuracy and stability are crucial.

In this work, with the aim of understanding the role of quenching and activation energy processes in the quenching mechanism of CDs fluorescence intensity by silver (AgNPs) have been studied. The fluorescence assay contains a CDs, which serves as a signal indicator due to its known photophysical properties. CDs and AgNPs were immobilized by adding amine- and thiol-modified oligonucleotide at the *5*'- and *3*'-end, respectively, thus increasing their coordination ability and sensitivity. As a strong molecular interaction pair, CDs-AgNPs forms a stable non-fluorescent complex with increasing concentration of target oligonucleotide. Furthermore, it is notable when the method is straightforward and affordable with a simple experimental protocol. In addition, CDs-AgNPs has never been reported as a fluorescence sensor for the detection of *E. coli* O157:H7.

MATERIALS AND METHODS

Chemicals and materials

Primer Premier 5.0 software was used to design DNA oligonucleotide obtained through *E. coli* DNA sequences in a published gene bank. In this study, six DNA sensor probes were designed to develop a sensing system against the *fliC* gene. All DNA oligonucleotides were synthesized and purified by an appointed company; Integrated DNA Technologies (IDT) Inc. (Singapore). All DNA oligonucleotides are made ready for laboratory use and store at −20 °C until used. *N*-hydroxysuccinimide (NHS), Tris(2-carboxyethyl)phosphine hydrochloride (TCEP), 1-ethyl-3-(3-dimethyl-aminopropyl) carbodiimide (EDC) and silver nanoparticles (AgNPs) with diameter 20 nm (OD 1) were obtained from Sigma-Aldrich (United States). The CDs were synthesized according to Zhu *et al*., [15] with some modifications. The oligonucleotides sequences used in this study are shown in Table 1.

Table 1. List of oligonucleotides, genes and primers used in this study

Oligo/Primer	**Sequence (*5*' to *3*')**	**Size (bp)**
Thiol modified	*5′*-CGTAGATTAT/**3ThioMC3-D**/*-3′*	10
Amine modified	*5′*-/**5AmMC6**/CAGTTGGCGG-*3′*	10
Complementary target	ATAATCTACGCCGCCAACTG	20
Target	ATAATCTACGCCGCCAACTG	20
One-base mismatch	ATAATCTA**T**GCCGCCAACTG	20
Two-base mismatch	ATAATCTA**T**GCCGC**G**AACTG	20
fliC gene	Region: 2719892 to 2720272	381
Forward primer (*fliC*)	ATAATCTACGCCGCCAACT	19
Reverse primer (*fliC*)	GACTCCATCCAGGACGAAA	19

Functionalization of CDs with -COOH

The previous method reported by Zhu *et al*., [15] was followed to synthesize CDs with some modifications. Citric acid weight of 5 g and ethylenediamine volume of 3125 µL was mixed in 50 mL ultra pure water. Then the mixture was pourred into a round bottom flask and heated at 150 °C for 5 hrs using reflux method. To retain and obtain the molecular weight of 3.5 kDa and nano size of CDs, the product was dialysed against the ultra pure water. The hydroxyl, epoxide and ester groups of the CDs were converted into COOH groups by mixing the 30 mg of CDs with 30 mL of basic solution containing 1.5 g of NaOH and 1.5 g of $ClCH_2COONa$ and bath sonicate for 3 hrs [16]. To obtain CDs-COOH, HCl was titrated to neutralize the CDs-COONa and followed by dialysis. Finally, a rotary evaporator was used to condense the as-developed CDs-COOH and followed by 3 days of freeze drying to obtain CDs-COOH in powder form.

Conjugation of CDs-COOH with amine oligonucleotide

The CDs-amine modified was produced by the carbodiimide crosslinking method [17]. Briefly, PBS with pH of 7.5 and concentration of 10 mM was added with 2 mg powder of CDs-COOH to acquire a CDs-COOH solution with 2 mg/mL concentration. Then 67.5 µL of 400 mM EDC and 81 µL of 400 mM NHS were pipetted to 1 mL of

CDs-COOH (2 mg/mL) solution and was bath sonicated for 2 hours. Next, 57 µL amine oligonucleotide (100 µM) was added to prepare the 5.7 µM working solution and followed by incubation for 24 hours at 4 °C. Then, the CDs-amine modified was kept at 4 °C until utilized.

Preparation of AgNPs-thiol modified

Thiol oligonucleotide (100 µM) were activated by adding a 100× excess of 10 mM tris(2-carboxyethyl) phosphine hydrochloride (TCEP), pH 8.2. The mixture was left for 2 hours at room temperature to reduce the disulfide bonds in preparation for silver (AgNPs) modification with thiol oligonucleotide. Then the mixture was left for not less than 18 hours at room temperature, immediately after TCEP-treated oligonucleotide (50 µM) in 40 µL was mixed with AgNPs solution in 1000 µL. Afterwards, 1× PBS (10 mM) was added in a dose of 122 µL to increase ionic strength and pH was adjusted to 7.4. After 6 hours of incubation, three increases of 21 µL of 2 M NaCl at 3 hours of gaps was added to enhance the NaCl concentration of the solution slowly. Then the mixture was incubated for 48 hours. To isolate the AgNPs-thiol modified conjugate, it was centrifuged for 15 min at 15,000 rpm and 14 °C. Then, it was washed twice with pH 7.4 of 0.1 M PBS and redispersed in the same concentration and pH of PBS.

Characterization of nanomaterials

High Resonance Transmission Electron Microscope (HRTEM) and energy-dispersive X-ray (EDX)

The morphological, particle size and elemental analysis was performed using High Resonance Transmission Electron Microscope (HRTEM) (JEM-2100F, JOEL, Japan) and energy-dispersive X-ray (EDX) (AZtec, Oxford Instruments, England) spectroscopy. TEM sample was prepared by dropping 10 µL of nanoparticle solution onto the carbon coated copper grid. Then the grid was left overnight through air drying and the next day is viewed under TEM. The same sample preparation was used for EDX imaging.

Fourier Transform Infra-Red (FTIR) spectroscopy

To observe the functional groups attached on the prepared nanomaterials, GQDs, CDs, AuNPs and AgNPs were characterized using the Fourier Transform Infra-Red (FTIR) (Spectrum 100, Perkin Elmer, United State). Nanomaterials were prepared in solid powder form. Then the sample were each directly placed onto the Attenuated Total Reflectance (ATR) accessory and scanned for 64 times from 4000 cm^{-1} to 550 cm^{-1}.

Fluorescence assay

Figure 1 show the mechanism that occur as a response of the developed system towards a series of target oligonucleotide was studied with a predetermined volume (50 µL, 5.7 µM) of fluorophore (F) solution. In order for hybridization to participate, the fluorophore solution was left for 2 hours at ambient temperature in 10 µL target oligonucleotide with a series dilution of 0.001 nM to 200 nM. For the next 20 minutes, 50 µL of quencher (Q) solution (2 µM) was mixed with the above preparation and left at ambient temperature to create a ground-state non-fluorescent complex (F-Q complex). Shortly after stable complex formation has been achieved, signal changes will be detected

by the microplate reader of Synergy H1 Hybrid Multi-Mode (United States). Complete signal changes were discovered and monitored at excitation and emission light of 340 nm and 450 nm, respectively.

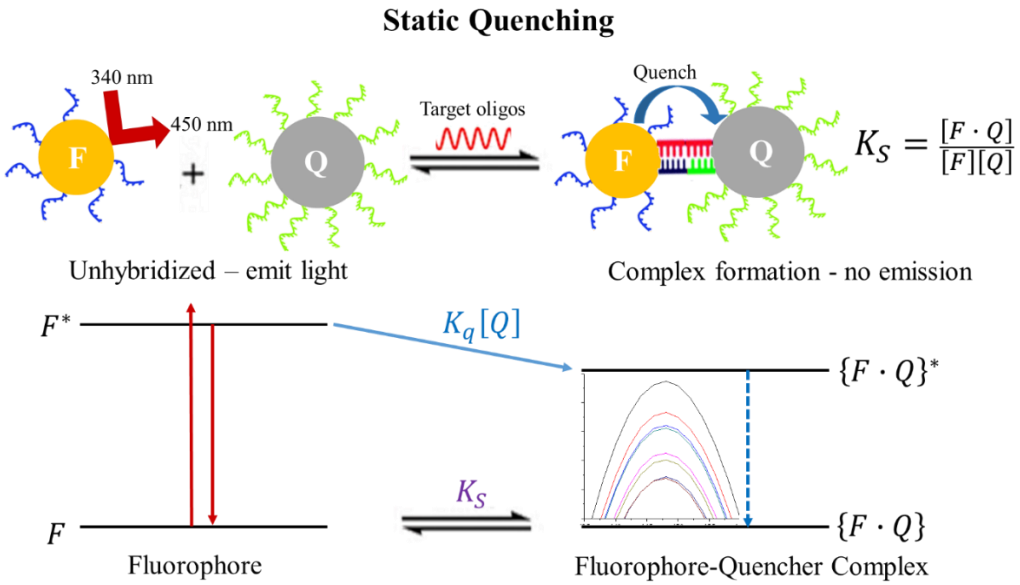

Figure 1. The mechanism that occurs as a response of the developed system towards a series of target oligonucleotide based on fluorescence assay.

RESULTS AND DISCUSSION

Characterization of nanoparticles

TEM-EDX

TEM-EDX (energy dispersive X-ray) analysis of the particles gives information about the size, formation and elemental presence of CDs-target-AgNPs nonfluorescent complex in the electron micrographs (50,000×) [7]. The TEM-EDX image of CDs-target-AgNPs nonfluorescent complex has shown that the morphology of CDs and AgNPs were predominantly spherical. The measured size of the CDs nanoparticle was 3.8 ± 0.2 nm. It is very clear that the AgNPs was distinct and spherical in contour with particle size of 23.9 ± 0.11 nm (Figure 2a). From EDX spectrum, it was clear that CDs-target-AgNPs nonfluorescent complex have percent yield of 98.68 ± 1.52% of Carbon (Figure 2b and 2c) and 1.32 ± 1.52% of Argentum (Figure 2d, 2e and 2f) [18].

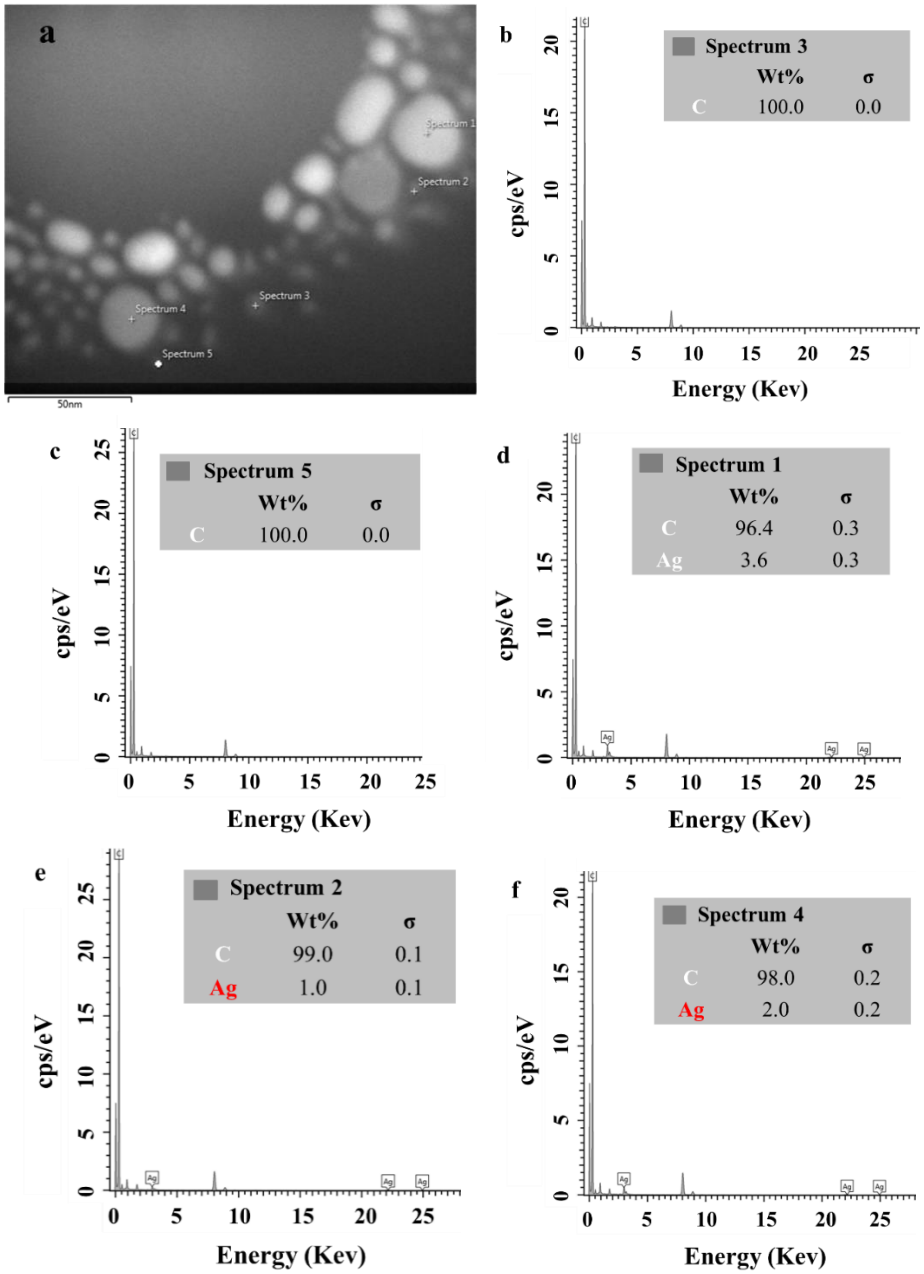

Figure 2. (a) TEM image of CDs-AgNPs in ground-state complex arrangement (50,000×) and EDX spectra of (b and c) CDs-amine modified and (d, e and f) AgNPs-thiol modified.

FTIR

To evaluate the successful functionalization of AgNPs, FTIR spectra were monitored, as depicted in Figure 3A. The effective functionalization of AgNPs with thiol, was indicated by the differences in the FTIR spectra of AgNPs-thiol modified compared to AgNPs spectrum. It is noted that the disappearance of weak S-S stretching vibrations (735 cm^{-1}) in AgNPs-thiol modified (Figure 3A(b)), which shows the deprotonation and formation of strong Ag-S covalent bond. Peaks associated to the S-H stretching bands

(2917 cm^{-1}) was formed in the FTIR spectra of AgNPs-thiol modified and absent in the FTIR spectra of AgNPs suggested the successful of thiol functionalization on AgNPs surface [19]. In addition, bands at 3300 cm^{-1}, 1560 cm^{-1} and 1386 cm^{-1} were associated to the O-H, C=C and C-H modes of carboxylic acids, alkene and alkane moieties on AgNPs (Figure 3A(a)) [10]. The FTIR spectra of CDs provide significant structural differences when compared with functionalized CDs and CDs-amine modified. In Figure 3B(a) the bands on the CDs-amine modified are markedly different from the functionalized CDs (Figure 3B(b)) and CDs (Figure 3B(c)) at 2973 cm^{-1}, 1637 cm^{-1}, 1565 cm^{-1} and 1241 cm^{-1}, respectively. In Figure 3B illustrates the obvious changes in the group region at the typical bands of C-NH-C (1070 cm^{-1}), C-O (1083 cm^{-1}) and NHC=O (1241 cm^{-1}). This clearly indicates that amine oligonucleotide was successfully conjugated on the CDs surface by forming amide bonds with carboxyl functional groups [20].

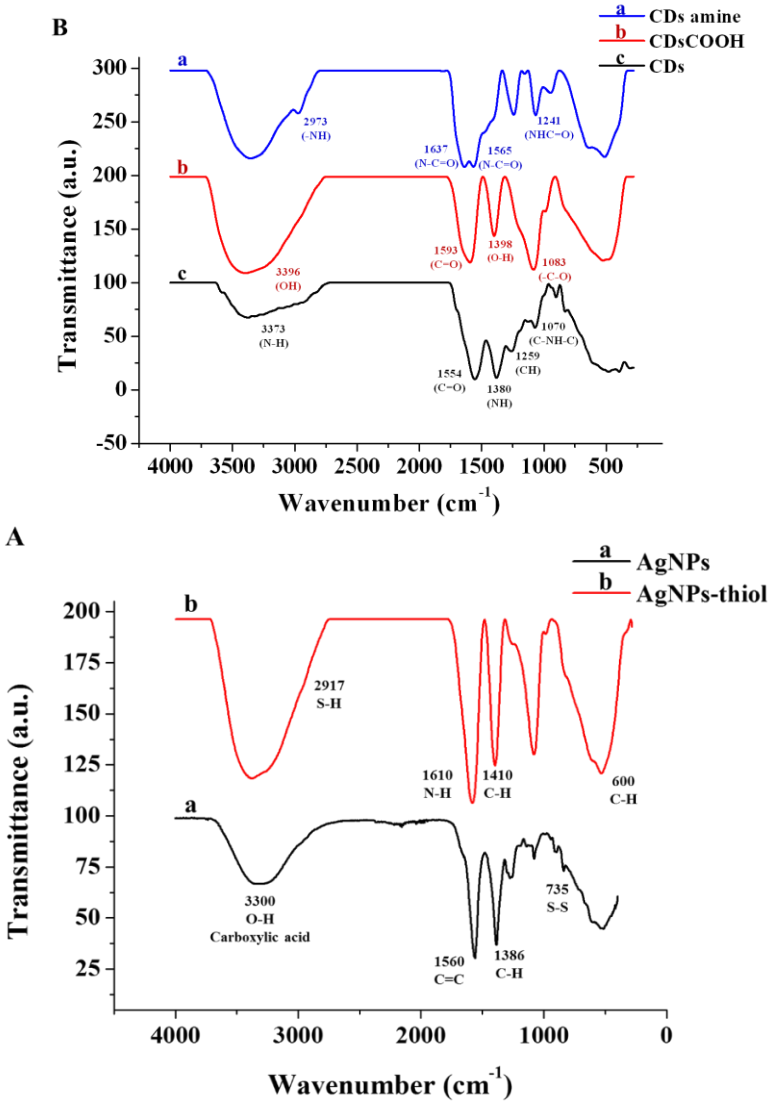

Figure 3. FTIR spectra of (A) (a) AgNPs and (b) AgNPs-thiol modified and (B) (a) conjugated CDs, (b) functionalized CDs and (c) carbon dots (CDs), respectively.

The optical spectrum of conjugated CDs and AgNPs

There was overlap between the conjugated CDs emission spectra with the conjugated AgNPs absorption spectra, thus demonstrating the feasibility of fluorescence quenching. As shown in Figure 4, fluorescence emission wavelength of CDs-amine modified particles at 450 nm has been overlapped with the absorption spectrum of the AgNPs-thiol modified particles at 400 nm. The overlapping spectra are important parameters to improve fluorescence quenching efficiency of the gene assay [21]. It can be concluded that they are a good fluorescence quenching pair based on the huge spectral overlap found between the fluorophore's emission and the quencher's absorption.

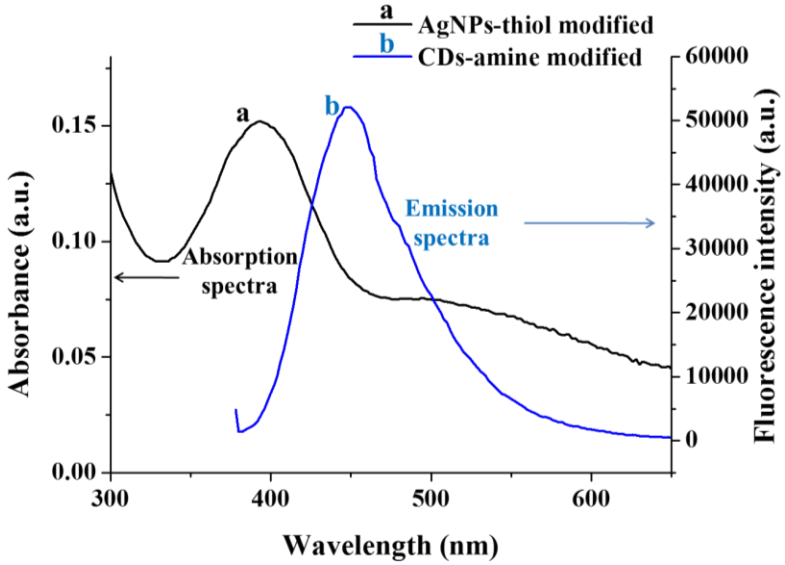

Figure 4. Spectra overlap between (a) CDs-amine modified and (b) AgNPs-thiol modified.

Optimum reaction time

To see the effect of reaction time on fluorescence quenching by the CDs-AgNPs fluorescence assay, the reaction time was carried out at 1 hour, 1.5 hours and 2.0 hours for hybridization (first incubation) and 10 min, 20 min, 30 min, 40 min, 50 min and 1 hour for co-hybridization (second incubation) by the adding of AgNPs-thiol modified to the CDs-target oligonucleotide mixture. As shown in Figure 5, an increase in incubation time will lead to a significant increase in the number of AgNPs-thiol modified that are close to the surface of CDs. These observations indicate that the CDs-amine modified sequence is in hybridization with the target oligonucleotide and then co-hybridized with the AgNPs-thiol modified before stabilizing the quenching effect on the CDs. The increase in fluorescence quenching by AgNPs reached the optimum level with an increase in hybridization time of up to 2 hours (first incubation) and co-hybridization time of up to 20 min (second incubation). After this point, the increase in incubation time with AgNPs-thiol modified did not increase the net fluorescence quenching of the reaction, indicating that a saturation state had been reached in the reaction. This is because additional targets have been fully co-hybridized with conjugated CDs and AgNPs, respectively. This observation is in agreement with the findings by Lin *et al*. [22] and Hai

et al. [23]**.** Thus, the 2 hours and 20 min of hybridization and co-hybridization time, respectively was chosen for further study.

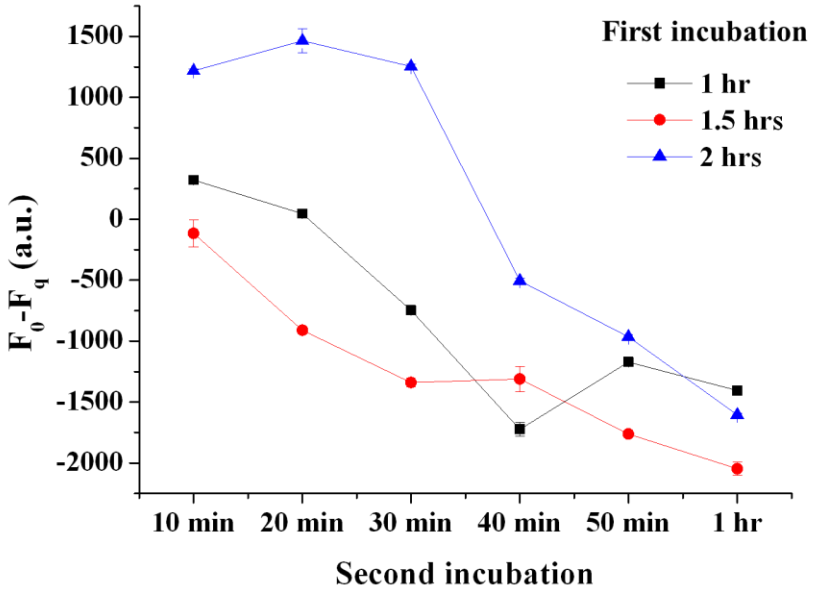

Figure 5. Optimum reaction time for CDs-AgNPs fluorescence assay.

Fluorescence quenching for target gene detection

Method validation

Under the optimum conditions, the fluorescence spectra of the CDs-AgNPs fluorescence assay at different concentrations of target oligonucleotide were studied. Figure 6a shows the response of the CDs-AgNPs fluorescence quenching system by increasing the target oligonucleotide concentrations in the range of 0.001 - 200 nM. The reduction of fluorescence signal due to the quenching effect of AgNPs on the CDs is in correlation with the concentrations of target oligonucleotide. It was observed that the strong fluorescence of the CDs-amine modified particles was gradually quenched with the increase of target concentrations. The results show that throughout the range of concentrations studied, CDs exhibit static quenching behaviour of Stern-Volmer quenching reaction. This is proven when there is no shift in the maximum emission wavelength observed, even for the high concentration of target oligonucleotide [24]. Figure 6b demonstrate the net fluorescence quenching of the as-prepared biosensor. This shows a linear relationship with the increase in target oligonucleotide concentration ranging from 0.001 - 200 nM (Figure 6b). CDs showed static quenching activities in the whole dynamic range analysed as showed by the changed of the performance of the Stern-Volmer quenching reaction in the presence of the target oligonucleotide. It was found that the wavelength maximum of emission was not shifted, although for immense concentrations of target oligonucleotide. Therefore, the reaction mixture maintains a static quenching process in the existence of target oligonucleotide whereas the dynamic quenching arrangement was overcame [24]. The calibration plot could be expressed by the equation:

$$F_0 - F_q = 240.36\,x + 1040.8 \qquad (2)$$

with the correlation coefficient of 0.896 (where, F_0 and F_q represented the emission intensities of the biosensor at 0 min and 20 min after adding of AgNPs-thiol modified, respectively). Data treatment with concentration logarithms in the calibration plot abscissa was not used to calculate the detection limit (LOD) based on calibration function slope as this resulted in a poor statistical evaluation [25]. The limit of detection (LOD) was calculated to be 0.0088 ± 0.71 nM, according to three times of standard deviation, 3*Sa*/*b* (*n* = 3) where *Sa* and *b* denote the blank standard deviation and the calibration plot slope. Compared with other reported literatures by Xu *et al*., [26], Achadu *et al*., [27], Yan *et al*., [28], Zhao *et al*., [29] and Sidhu *et al*., [30], the CDs-AgNPs fluorescence assay provides a relatively lower detection limit and broader dynamic range (Table A.1, supplementary data/appendix).

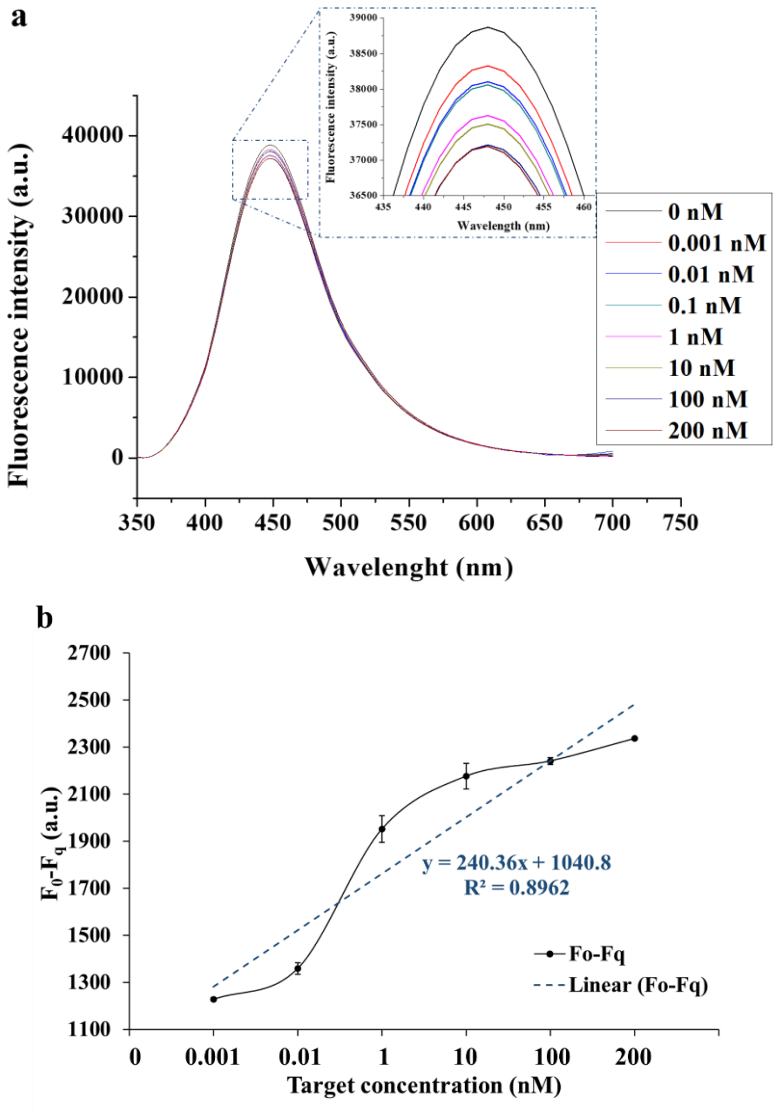

Figure 6. (a) Fluorescence spectra and (b) calibration plot for quantification of target oligonucleotide in the dynamic range of 0.001 to 200 nM of CDs-AgNPs fluorescence assay.

Stern-Volmer constant (Ksv)

The fluorescence intensities were measured with and without quencher concentrations for the CDs-amine modified. The fluorescence intensity decreases with increasing AgNPs concentrations. Figure 7 shows the Stern-Volmer plot derived from equation [1] of CDs fluorescence quenching using AgNPs as quencher (Q). F^o and F are the fluorescence intensities without and with of the quencher concentration [AgNPs]. The K_{SV} was calculated as 6.5×10^5 M^{-1} in CDs-AgNPs. This indicated that AgNPs is a strong electron acceptor, compatible with its being a notably effective quencher [31]. The Stern-Volmer plots shows that fluorescence quenching follows the Stern-Volmer association and confirmed the static quenching contribution. The static quenching constant (K_S), given by the slope of the Stern-Volmer plots, were measured using least squares method [32].

The quenching efficiency increases as the mixture concentration increases indicating that the quenching process is not completely diffusion-controlled. This is in accordance with a static quenching model in which enhancing the medium concentration result in a confine effect that boosts fluorophore uptake on AgNPs surfaces [33]. Data on Stern-Volmer plot for CDs-AgNPs fluorescence assay are summarized in Table A.2, supplementary data/appendix.

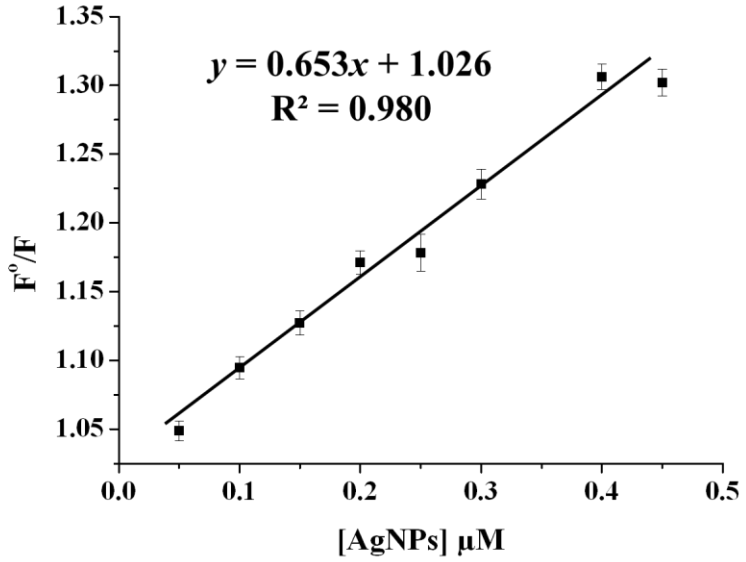

Figure 7. Stern-Volmer plot of fluorescence quenching of CDs-amine modified by AgNPs-thiol modified.

Association constant (K_a)

The effect of AgNPs concentration on the absorption of CDs molecule was also studied by Benesi-Hildebrand equation as specified in equation 3:

$$\frac{1}{F^{\circ}-F} = \frac{1}{\Delta\varepsilon} + \frac{1}{K_a} \times \frac{1}{(\Delta\varepsilon)[Q]} \qquad (3)$$

Where F^o and F are fluorescence intensity with and without quencher (AgNPs), $\Delta\varepsilon$ is the change in absorption coefficient, K_a is association constant and $[Q]$ is the concentration of AgNPs. The plot (Figure 8) was discovered to be linear with excellent

correlation factor (R^2 = 0.99). The association constant K_a is 2.5 × 10^6 M^{-1} (Figure 8) as determined from the slope of the plot and *y*-intercept. This shows that there is a strong relation between AgNPs and the CDs molecule [34]. Data on Benesi-Hildebrand plot for CDs-AgNPs fluorescence assay are summarized in Table A.3, supplementary data/appendix.

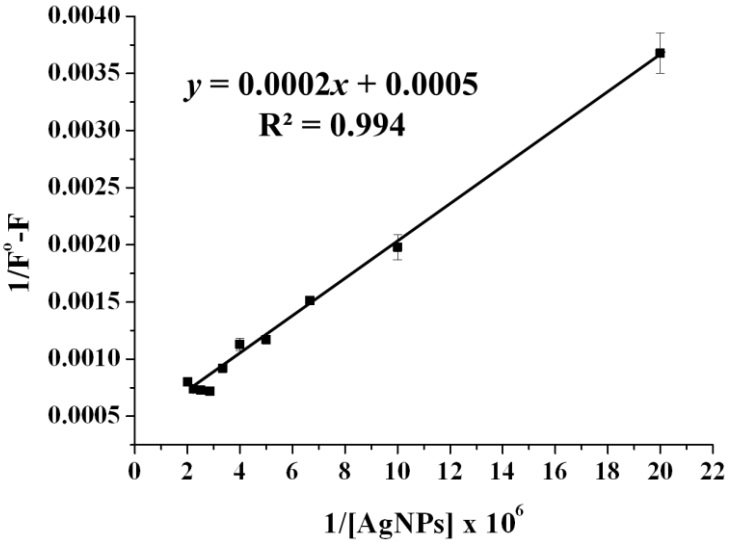

Figure 8. Benesi-Hildebrand plot for the adsorption of CDs-amine modified on AgNPs-thiol modified.

Equilibrium binding constant and number of binding sites

The equilibrium binding constant (K_A) and binding sites (n) can be presented as:

$$\log\left[\frac{(F°-F)}{F}\right] = \log K_A + n\log[Q] \qquad (4)$$

Where F^o, F and [Q] are the same as in Equation (3), K_A is the equilibrium binding constant and n is the binding sites. By using the plot of log[(F^o−F)/F] versus log[Q] as shown in Figure 9, the numbers of binding sites (n) of CDs-AgNPs is calculated to be 1.2, which is close to 1, indicates that there is one binding site between CDs and AgNPs. The equilibrium binding constants K_A is 1.7 × 10^6 M^{-1}. The large value of K_A indicated that there is a strong interaction between conjugated fluorophore (CDs) and quencher (AgNPs). The n values indicating that the stability of complex between CDs and AgNPs which represent the strength and number of energy transfer takes place within the CDs and AgNPs complex [35]. Data on log [(F^o−F)/F] vs log [Q] plot for CDs-AgNPs fluorescence assay are summarized in Table A.4, supplementary data/appendix.

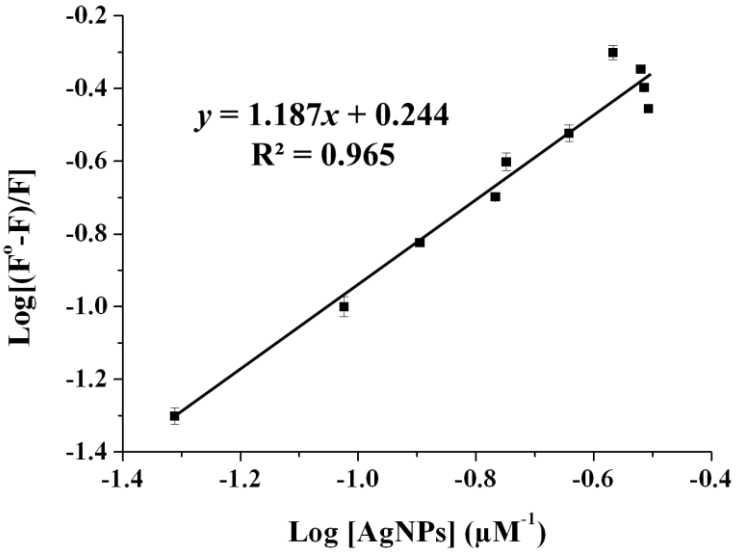

Figure 9. Plot of log [(F^o−F)/F] vs log [AgNPs]-thiol modified.

Specificity and selectivity of CDs-AgNPs fluorescence assay

To evaluate the specificity of the CDs-AgNPs fluorescence assay, specific identification of *E. coli* O157:H7 *fliC* gene compared to other bacteria strain, *Salmonella enteritidis* (*S. enteritidis*) and *Salmonella typhimurium* (*S. typhimurium*) was analysed. As illustrated in Figure 10a, CDs fluorescence quenching was strongly driven by increased in genomic DNA, and no other bacterial strain resulted in similar changes in fluorescence intensity at concentrations similar to *E. coli* O157:H7 genomic DNA. Notably, although there was a similarity of target concentrations (1.7×10^5 DNA copy number) it did not give the same effect on CDs fluorescence intensity. Thus, showing that the presence of other bacteria does not interfere with the detection of the target sequence. These findings clearly indicate that the specificity of the proposed fluorescence sensor system for the *fliC* gene is acceptable. Figure 10a shows that CDs-AgNPs was efficient in specific identification of *fliC* gene. The quenching efficiency of CDs-AgNPs in detecting *fliC* gene for *E. coli* O157:H7, *S. enteritidis* and *S. typhimurium* were 97.18 ± 1.50%, 26.51 ± 5.04% and 30.22 ± 4.88%, respectively.

To exhibit the selectivity of proposed method, target analytes in different type of target sequences were also examined. The concentration of target oligonucleotide was set at 200 nM for each type of target sequences and determined by the CDs-AgNPs fluorescence assay. Figure 10b shows that CDs-AgNPs was efficient in selective detection of *fliC* gene. The quenching efficiency of CDs-AgNPs in detecting *fliC* gene for complementary, one mismatch and two mismatches sequence were 96.33 ± 1.41%, 79.81 ± 2.45% and 64.04 ± 6.46%, respectively.

Thus, the CDs-AgNPs sensing system can embrace potential applications for the determination of *fliC* gene in real samples analysis with a better behavior as previously demonstrated.

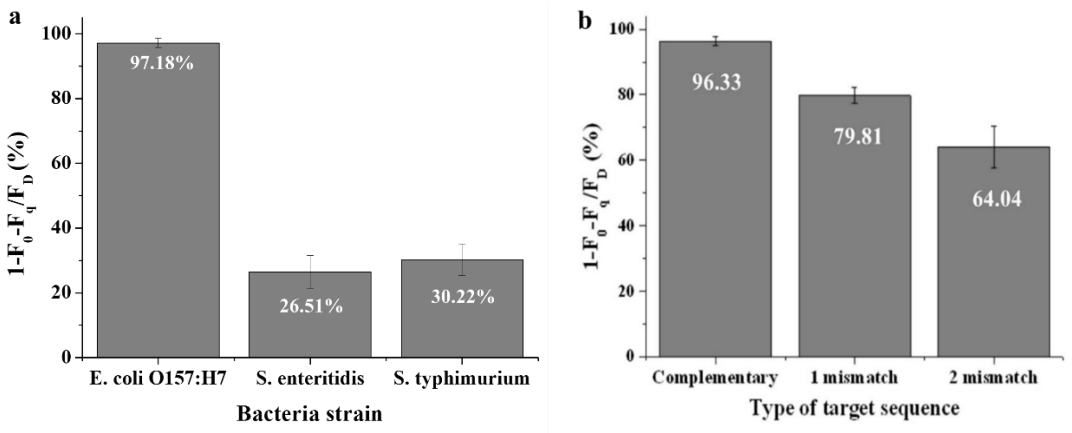

Figure 10. Quenching efficiency (∑) of CDs-AgNPs fluorescence assay towards (a) different bacteria strain and (b) type of target sequence.

Application in actual samples

The capability to identify *E. coli* O157:H7 in actual samples was evaluated to confirm the on-field application of the developed system. To achieve this, *E. coli* O157:H7 was spiked into several food samples in certain amounts. The result of the actual sample application was shown in Figure 11 with a linear plot of net fluorescence quenching ($F_0 - F_q$) against serially diluted amplicon (*fliC* gene). A direct proportion was obtained with a series dilution of 0.05 ng/μL to 500 ng/μL of amplicon. The linear plot was projected by the equation of $y = 323.05x - 44.55$ ($R^2 = 0.984$). The system detection limit (LOD) in the actual samples identification is 0.07 ± 0.71 ng/μL for $n = 3$. The actual samples shown in Table 2 were confirmed to be positive with an average concentration of *fliC* gene 2.62 ± 0.11 ng/μL in chicken, 10.94 ± 0.20 ng/μL in meat and 41.78 ± 0.04 ng/μL in cheese. The data of PCR is significantly lower than that obtained with the proposed fluorescent sensors for the sample of chicken. This is due to the effect of steric hindrance where low target concentrations reduce the probability of co-hybridization of target sequences with amine and thiol oligonucleotide on CDs and AgNPs. In addition, target secondary structure, type (RNA or DNA) and length also affect hybridization, probe-target duplex formation competencies and specificity [36]. A common technique in molecular biology to measure the number of DNA molecules is real time PCR [37]. Thus, real time PCR validation was used as a comparison against the data obtained from the developed fluorescence assay (Table 2).

The two population means of the fluorescence assay and the real time PCR method was compared in statistical analysis to calculate the *t*-test value (Table 2). A *t*-test value that smaller than the critical value ($t_4 = 2.78$) confirmed the fluorescence assay was comparable and in good agreement with the real time PCR method. The results obtained further reinforce the fact that the CDs-AgNPs system has the potential for real testing when successfully detecting the *fliC* gene accurately and effectively in actual samples.

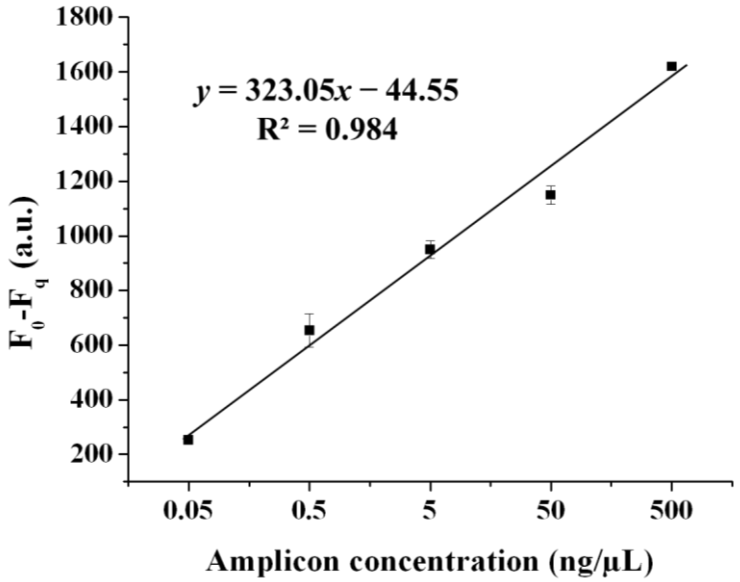

Figure 11. Calibration plot of *fliC* gene (amplicon) serial dilution in the dynamic range of 0.00 - 500.00 ng/µL (n = 3).

Table 2. Data on CDs-AgNPs fluorescence assay and real time PCR method

Food sample	CDs-AgNPs (ng/µL)	Real time PCR (ng/µL)	*t*-test
Chicken	2.62 ± 0.11	0.045 ± 0.001	1.96
Meat	10.94 ± 0.20	10.14 ± 0.02	0.35
Cheese	41.78 ± 0.04	41.90 ± 0.07	0.31

Note: [a] the critical value, t_4 = 2.78 (p = 0.05)

CONCLUSION

An unlabeled fluorescent-based method exploiting fluorescent carbon dots and silver nanoparticles was developed and used for the sensitive and selective detection of *fliC* gene. In brief, a label-free fluorescence-based method utilizing luminescent carbon dots was developed for the identification of *E. coli* O157:H7 *fliC* gene. AgNPs was found to effectively quench the emission of CDs in the presence of target. A probable process for this fluorescence quenching engages absorption from the CDs to AgNPs created by the non-fluorescent complex formation of CDs-AgNPs following co-hybridization of target oligonucleotide. The presented sensing mechanism has several properties. First, the method is straightforward and affordable with easy experimental protocols. Second, the assay do not require complex modification steps and gives high specificity and sensitivity. Furthermore, synthesized CDs are minimal toxic and should be valuable for actual sample applications.

SUPPLEMENTARY DATA

Supplementary data to this article can be found in Appendix A.

ACKNOWLEDGEMENT

The authors want to appreciate Universiti Putra Malaysia (UPM) and MARDI for sponsoring the research fund. Last but not least, thanks to Jabatan Perkhidmatan Awam (JPA) for the scholarship through Hadiah Latihan Persekutuan (HLP).

REFERENCES

[1] V. Mishra, A. Patil, S. Thakur, and P. Kesharwani, "Carbon dots: emerging theranostic nanoarchitectures," *Drug Discov. Today*, vol. 23, no. 6, pp. 1219–1232, 2018, doi: 10.1016/j.drudis.2018.01.006.

[2] J. Saha, A. Datta Roy, D. Dey, D. Bhattacharjee, and S. Arshad Hussain, "Role of quantum dot in designing FRET based sensors," *Mater. Today Proc.*, vol. 5, pp. 2306–2313, 2018, doi: 10.1016/j.matpr.2017.09.234.

[3] X. Sun and Y. Lei, "Fluorescent carbon dots and their sensing applications," *Trends Anal. Chem.*, vol. 89, pp. 163–180, 2017, doi: 10.1016/j.trac.2017.02.001.

[4] H. Li, Z. Kang, Y. Liu, and S. T. Lee, "Carbon nanodots: Synthesis, properties and applications," *J. Mater. Chem.*, vol. 22, no. 46, pp. 24230–24253, 2012, doi: 10.1039/c2jm34690g.

[5] J. Kim, M. A. A. Mohamed, K. Zagorovsky, and W. C. W. Chan, "State of diagnosing infectious pathogens using colloidal nanomaterials," *Biomaterials*, vol. 146, pp. 97–114, 2017, doi: 10.1016/j.biomaterials.2017.08.013.

[6] F. G. Wouterlood and A. J. Boekel, "Fluorescence Microscopy in the Neurosciences," in *Encyclopedia of Neuroscience*, Amsterdam, The Netherlands: Academic Press, 2009, pp. 253–260. doi: 10.1016/B978-008045046-9.00666-5.

[7] X. F. Zhang, Z. G. Liu, W. Shen, and S. Gurunathan, "Silver nanoparticles: Synthesis, characterization, properties, applications, and therapeutic approaches," *Int. J. Mol. Sci.*, vol. 17, pp. 1–34, 2016, doi: 10.3390/ijms17091534.

[8] S. H. Lee and B. H. Jun, "Silver nanoparticles: Synthesis and application for nanomedicine," *Int. J. Mol. Sci.*, vol. 20, pp. 1–24, 2019, doi: 10.3390/ijms20040865.

[9] D. Ghosh and N. Chattopadhyay, "Gold and silver nanoparticles based superquenching of fluorescence: A review," *J. Lumin.*, vol. 160, pp. 223–232, 2015, doi: 10.1016/j.jlumin.2014.12.018.

[10] A. Pani, J. H. Lee, and S. I. Yun, "Autoclave mediated one-pot-one-minute synthesis of AgNPs and Au-Ag nanocomposite from Melia azedarach bark extract with antimicrobial activity against food pathogens," *Chem. Cent. J.*, vol. 10, pp. 1–11, 2016, doi: 10.1186/s13065-016-0157-0.

[11] C. Wang *et al.*, "Novel ELISA based on fluorescent quenching of DNA-stabilized silver nanoclusters for detecting E. coli O157:H7," *Food Chem.*, vol. 281, pp. 91–96, 2019, doi: 10.1016/j.foodchem.2018.12.079.

[12] K. Flynn *et al.*, "An introduction to current food safety needs," *Trends Food Sci. Technol.*, vol. 84, pp. 1–3, 2019, doi: 10.1016/j.tifs.2018.09.012.

[13] B. M. T. Shamsul, M. T. Adamu, M. N. Mohd Desa, and S. Khairani-Bejo, "Prevalence of Escherichia coli O157:H7 and Enterobacteriaceae on hands of workers in halal cattle abattoirs in peninsular Malaysia," *Malaysian J. Med. Sci.*, vol. 23, no. 5, pp. 65–71, 2016, doi: 10.21315/mjms2016.23.5.9.

[14] B. Pang *et al.*, "Development of a low-cost paper-based ELISA method for rapid Escherichia coli O157:H7 detection," *Anal. Biochem. 542*, vol. 542, pp. 58–62, 2017, doi: 10.1016/j.ab.2017.11.010.

[15] S. Zhu *et al.*, "Highly photoluminescent carbon dots for multicolor patterning, sensors, and bioimaging," *Angew. Chemie - Int. Ed.*, vol. 52, no. 14, pp. 3953–3957, 2013, doi: 10.1002/anie.201300519.

[16] L. Zhang, J. Xia, Q. Zhao, L. Liu, and Z. Zhang, "Functional graphene oxide as a nanocarrier for controlled loading and targeted delivery of mixed anticancer drugs," *Small*, vol. 6, no. 4, pp. 537–544, 2010, doi: 10.1002/smll.200901680.

[17] Z. S. Qian, X. Y. Shan, L. J. Chai, J. J. Ma, J. R. Chen, and H. Feng, "DNA nanosensor based on biocompatible graphene quantum dots and carbon nanotubes.," *Biosens. Bioelectron.*, vol. 60, pp. 64–70, Oct. 2014, doi: 10.1016/j.bios.2014.04.006.

[18] T. Fafal, P. Taştan, B. S. Tüzün, M. Ozyazici, and B. Kivcak, "Synthesis, characterization and studies on antioxidant activity of silver nanoparticles using Asphodelus aestivus Brot. aerial part extract," *South African J. Bot.*, vol. 112, no. September, pp. 346–353, 2017, doi: 10.1016/j.sajb.2017.06.019.
[19] K. Chandraker, S. K. Vaishanav, R. Nagwanshi, and M. L. Satnami, "Radical Scavenging Efficacy of Thiol Capped Silver Nanoparticles," *J. Chem. Sci.*, vol. 127, no. 12, pp. 2183–2191, 2015, doi: 10.1007/s12039-015-0968-x.
[20] J. Shangguan *et al.*, "Highly Fe3+-Selective Fluorescent Nanoprobe Based on Ultrabright N/P Codoped Carbon Dots and Its Application in Biological Samples," *Anal. Chem.*, vol. 89, no. 14, pp. 7477–7484, 2017, doi: 10.1021/acs.analchem.7b01053.
[21] G. Tang, L. Du, and X. Su, "Detection of melamine based on the fluorescence resonance energy transfer between CdTe QDs and Rhodamine B," *Food Chem.*, vol. 141, pp. 4060–4065, 2013, doi: 10.1016/j.foodchem.2013.06.135.
[22] X. Lin, X. Hai, N. Wang, X. W. Chen, and J. H. Wang, "Dual-signal model array sensor based on GQDs/AuNPs system for sensitive protein discrimination," *Anal. Chim. Acta*, vol. 992, pp. 105–111, 2017, doi: 10.1016/j.aca.2017.09.006.
[23] X. Hai, X. Lin, X. Chen, and J. Wang, "Highly selective and sensitive detection of cysteine with a graphene quantum dots-gold nanoparticles based core-shell nanosensor," *Sensors Actuators B Chem.*, vol. 257, pp. 228–236, 2018, doi: 10.1016/j.snb.2017.10.169.
[24] G. Hollett *et al.*, "Quantum Ensembles of Silicon Nanoparticles: Discrimination of Static and Dynamic Photoluminescence Quenching Processes," *J. Phys. Chem. C*, vol. 123, no. 29, pp. 17976–17986, 2019, doi: 10.1021/acs.jpcc.9b04334.
[25] P. L. Urban, "Please Avoid Plotting Analytical Response against Logarithm of Concentration," *Anal. Chem.*, vol. 92, no. 15, pp. 10210–10212, 2020, doi: 10.1021/acs.analchem.0c02096.
[26] Z. Xu, P. Deng, J. Li, L. Xu, and S. Tang, "Molecularly imprinted fluorescent probe based on FRET for selective and sensitive detection of doxorubicin," *Mater. Sci. Eng. B*, vol. 218, pp. 31–39, 2017, doi: 10.1016/j.mseb.2017.02.005.
[27] O. J. Achadu and T. Nyokong, "Graphene quantum dots anchored onto mercaptopyridine-substituted zinc phthalocyanine-Au@Ag nanoparticle hybrid: Application as fluorescence 'off-on-off' sensor for Hg2+and biothiols," *Dye. Pigment.*, vol. 145, pp. 189–201, 2017, doi: 10.1016/j.dyepig.2017.06.002.
[28] F. Yan *et al.*, "Fluorescent carbon dots for ratiometric detection of curcumin and ferric ion based on inner filter effect, cell imaging and PVDF membrane fouling research of iron flocculants in wastewater treatment," *Sensors Actuators, B Chem.*, vol. 287, pp. 231–240, 2019, doi: 10.1016/j.snb.2019.01.144.
[29] J. Zhao, L. Zhao, C. Lan, and S. Zhao, "Graphene quantum dots as effective probes for label-free fluorescence detection of dopamine," *Sensors Actuators, B Chem.*, vol. 223, pp. 246–251, 2016, doi: 10.1016/j.snb.2015.09.105.
[30] J. S. Sidhu, A. Singh, N. Garg, N. Kaur, and N. Singh, "Gold conjugated carbon dots nano assembly: FRET paired fluorescence probe for cysteine recognition," *Sensors Actuators, B Chem.*, vol. 282, pp. 515–522, 2019, doi: 10.1016/j.snb.2018.11.105.
[31] M. Carpes Nunes *et al.*, "Turn-on fluorescence study of a highly selective acridine-based chemosensor for Zn2+ in aqueous solutions," *Inorganica Chim. Acta*, vol. 499, p. 119191, 2020, doi: 10.1016/j.ica.2019.119191.
[32] X. Wang *et al.*, "Photoinduced electron transfers with carbon dots," *Chem. Commun.*, vol. 25, pp. 3774–3776, 2009, doi: 10.1039/b906252a.
[33] S. A. El-Daly, M. M. Rahman, K. A. Alamry, and A. M. Asiri, "Fluorescence quenching of N,N-bis(2,5-di-tert-butylphenyl)-3,4:9,10- perylenebis(dicarboximide) (DBPI) by silver nanoparticles," *J. Lumin.*, vol. 148, pp. 303–306, 2014, doi: 10.1016/j.jlumin.2013.12.026.
[34] P. Kundu and N. Chattopadhyay, "Exogenous delivery of a pyrazole based bioactive probe to natural DNA through non-ionic TX-165 micellar carrier," *J. Drug Deliv. Sci. Technol.*, vol. 49, no. October 2018, pp. 413–419, 2019, doi: 10.1016/j.jddst.2018.12.007.
[35] L. S. Walekar, P. Hu, H. Vafaei Molamahmood, and M. Long, "FRET based integrated pyrene-AgNPs system for detection of Hg (II) and pyrene dimer: Applications to environmental analysis," *Spectrochim. Acta - Part A Mol. Biomol. Spectrosc.*, vol. 198, pp. 168–176, 2018, doi: 10.1016/j.saa.2018.03.012.
[36] W. T. Liu, H. Guo, and J. H. Wu, "Effects of target length on the hybridization efficiency and

specificity of rRNA-based oligonucleotide microarrays," *Appl. Environ. Microbiol.*, vol. 73, no. 1, pp. 73–82, 2007, doi: 10.1128/AEM.01468-06.

[37] T. S. Kang, "Basic principles for developing real-time PCR methods used in food analysis: A review," *Trends Food Sci. Technol.*, vol. 91, pp. 574–585, 2019, doi: 10.1016/j.tifs.2019.07.037.

APPENDIX A

Table A.1. Comparison with previous reported work on fluorescence based sensor

Nanomaterials	Technique	LOD (nM)	Reference
CDs	FRET	13.8	[25]
PEI-GQDs-Au@Ag	Fluorescence off-on-off	2.45	[26]
CDs	Fluorescence ratiometric	18.1	[27]
GQDs	Label-free fluorescence	90.0	[28]
CDs/Cys and Au	FRET	5.0	[29]
CDs and AgNPs	Fluorescence quenching	1.01	This work

Table A.2. Data on Stern-Volmer plot of CDs-AgNPs based fluorescence assay

[AgNPs] µM	F^o	F	F^o/F	RSD
0.05	5845	5573	1.05	0.007325
0.10	5845	5340	1.09	0.007935
0.15	5845	5185	1.13	0.008736
0.20	5845	4991	1.17	0.008624
0.25	5845	4960	1.18	0.013546
0.30	5845	4759	1.23	0.010939
0.40	5845	4475	1.31	0.009111
0.45	5845	4489	1.30	0.009633

Table A.3. Data on Benesi-Hildebrand plot of CDs-AgNPs based fluorescence assay

[AgNPs] µM	F^o	F	F^o-F	$1/F^o-F$	1/[AgNPs]	RSD
0.05	5845	5553	292	0.0034	20.00	0.000178
0.10	5845	5297	548	0.0018	10.00	0.00011
0.15	5845	5192	653	0.0015	6.67	1.15E-05
0.20	5845	4989	856	0.0012	5.00	1.93E-06
0.25	5845	5017	828	0.0012	4.00	5.5E-05
0.30	5845	4692	1153	0.0009	3.33	3.78E-05
0.35	5845	4418	1427	0.0007	2.86	1.43E-05
0.40	5845	4458	1387	0.0007	2.50	6.33E-06
0.45	5845	4488	1357	0.0007	2.22	3.84E-07
0.50	5845	4533	1312	0.0008	2.00	2.85E-05

Table A.4. Data on plot of log [(F^o−F)/F] vs log [AgNPs] of CDs-AgNPs based fluorescence assay

[AgNPs] µM	***F*^{o}**	***F***	***F*^{o}−*F***	***F*^{o}−*F*/*F***	**Log[(*F*^{o}−*F*)/*F*]**	**Log [AgNPs]**	**RSD**
0.05	5845	5573	272	0.0488	-1.3115	-1.30	0.022893
0.10	5845	5340	505	0.0946	-1.0242	-1.00	0.027577
0.15	5845	5185	660	0.1273	-0.8952	-0.82	0.003689
0.20	5845	4991	854	0.1711	-0.7667	-0.70	0.000841
0.25	5845	4960	885	0.1784	-0.7485	-0.60	0.023953
0.30	5845	4759	1086	0.2282	-0.6417	-0.52	0.022739
0.35	5845	4458	1387	0.3111	-0.5071	-0.46	0.011499
0.40	5845	4475	1370	0.3061	-0.5141	-0.40	0.004956
0.45	5845	4489	1356	0.3021	-0.5199	-0.35	0.000295
0.50	5845	4599	1246	0.2709	-0.5671	-0.30	0.020289